Ionization, excitation, protonium formation, and energy loss of antiprotons colliding with atomic hydrogen

R. Cabrera-Trujillo [1,2,*] C. E. de la C. Roman [1] and C. E. Teran-Cisneros [1]

[1]*Instituto de Ciencias Fisicas, Universidad Nacional Autonoma de Mexico, Ap. Postal 43-8, Cuernavaca, Morelos, 62251, Mexico*

[2]*Department of Physics, University of Gothenburg, SE-412 96 Goteborg, Sweden*

(Received 22 March 2023; accepted 11 July 2023; published 24 July 2023)

In this work, we investigate the collision process of antiprotons incidents on atomic hydrogen for energies in the range 0.003–900 keV. We solve the time-dependent Schrödinger equation, in a numerical lattice, for the electron by implementing a Crank-Nicholson implicit method. For the proton and antiproton, a classical description coupled to the quantum electron is proposed to obtain the electron-nuclear dynamics within a semiclassical impact parameter approach. The ionization process is treated by means of an absorbing masking function. We find that the absorbing layer induces an exponential behavior in the ionization process allowing one to determine the asymptotic ionization limit at large times. We assess the validity of the Fermi-Teller criteria for the ionization process at intermediate collision energies. At low collision energies the formation of protonium dominates the ionization process at small impact parameters, while at higher energies larger impact parameters contribute. Excitation probabilities into the $n = 2$ energy level of hydrogen are also reported. Finally, the total, electronic, and nuclear stopping cross sections are determined for collision energies above the closing of the protonium formation channel. The nuclear energy loss has a larger contribution than the electronic at low collision energies, as a consequence of the polarization induced by the antiproton on the hydrogen target. Good agreement is found when compared to available experimental data and other theoretical approaches.

DOI: 10.1103/PhysRevA.108.012817

I. INTRODUCTION

The LEAR [1,2], ASACUSA [3], and CERN PS194 collaborations [4–7] have trapped and cooled antiprotons for the study of matter-antimatter interactions in order to understand processes such as annihilation life times and formation cross sections. When an atom captures a long-lived heavy particle, like the antiproton, it becomes an exotic atom [8,9]. The simplest antiproton capture process is by substitution or ionization of an electron in the atom. Theoretically, the simplest and most appealing system to calculate the ionization cross sections is that of atomic hydrogen (or deuterium). Furthermore, antiproton projectiles are especially suited for tests of ionization theories because of their relatively large mass, which allows them to be treated in a semiclassical impact parameter approach. For example, antiprotonic helium has been studied extensively, both theoretically and experimentally [10]; however, it is a complicated three-body problem. The formation of the even simpler exotic system $p\bar{p}$, named protonium (Pn), has not been properly realized, even though high-resolution spectroscopy of Pn is of importance in the study of fundamental physical principles [11].

The reaction channels that appear in a collision of an antiproton with atomic hydrogen are

$$\bar{p} + \mathrm{H} \rightarrow \begin{cases} \mathrm{Pn} + e^- \\ \bar{p} + p + e^- \\ \bar{p} + \mathrm{H}^*, \end{cases} \tag{1}$$

where H^* is a hydrogen left in an excited state. For a review of the physics of antiprotonic systems, see Refs. [12,13]. Experimental and theoretical developments are also reviewed in detail by Kirchner and Knudsen [14]. Given the importance of this basic system, our current understanding of the dynamics of the protonium formation, excitation, ionization, and energy loss processes can be found in the literature [15–34]. However, much of that work is based on antiprotons straight-line trajectory approaches or the pseudocontinuum treatment of the ionization channel through a coupled channel approach suitable for high collision energies for electronic properties without accounting for the nuclei trajectories.

In this work we present calculations of the collision of antiprotons with atomic hydrogen targets with relative energies from 3 eV to 900 keV in the laboratory reference frame by accounting for the ionization process in a numerical lattice within an electron-nuclear dynamics approach. We report, and extend to lower collision energy, the ionization, excitation, protonium formation, and energy deposition of antiprotons colliding with atomic hydrogen in a lattice method without recurring to a basis set approach as done traditionally. We

*trujillo@icf.unam.mx

find that the nuclear stopping cross section dominates over the electronic at low collision energies.

The layout of our work is the following. In Sec. II, we present a summary of our theoretical approach based on a numerical solution to the Schrödinger equation that provides the dynamics of the electron coupled to that of the antiproton and proton. In Sec. III, we report the results of our study. We start with the ionization probability, followed by the excitations, protonium formation, antiproton energy loss, and nuclear energy gained by the hydrogen target. Finally, our conclusions are given in Sec. IV. Atomic units are used unless physical units are stated.

II. THEORY: LATTICE APPROACH

Following a similar treatment for coupling electrons and nuclei dynamics to the so-called time-dependent electron-nuclear dynamics (END) approach [35], the time-dependent Schrödinger equation for an electron in the presence of N nuclei is given by

$$i\frac{\partial}{\partial t}\Psi(\mathbf{r},t)=\left[-\frac{1}{2}\nabla^2+\sum_{i=1}^{N}\frac{Z_i}{|\mathbf{r}-\mathbf{R}_i(t)|}\right]\Psi(\mathbf{r},t), \qquad (2)$$

where $\Psi(\mathbf{r},t)$ is treated numerically in a space grid. In Eq. (2), Z_i is the charge of the ith nuclei and $\mathbf{R}_i$ is the heavy nuclei trajectory coupled to the electron through the equations

$$\dot{\mathbf{R}}_i=\frac{1}{M_i}\mathbf{P}_i(t)$$

$$\dot{\mathbf{P}}_i=Z_i\langle\Psi|\frac{(\mathbf{r}-\mathbf{R}_i)}{|\mathbf{r}-\mathbf{R}_i|^3}|\Psi\rangle-\sum_{k\neq i}^{N}Z_kZ_i\frac{(\mathbf{R}_k-\mathbf{R}_i)}{|\mathbf{R}_k-\mathbf{R}_i|^3}, \qquad (3)$$

where i runs from 1 to N number of heavy nuclei. In our case $N=2$.

Our lattice solution to Eq. (2) utilizes a uniform grid with a three-point finite-differences method within a Crank-Nicholson approach, as proposed in Ref. [36]. We treat the ionization by means of a masking function $M(\mathbf{r})$ at each time step in order to absorb the ionized electron through the grid boundary [37]. The masking function is implemented over a box Ω at the border of the numerical grid (space between the blue and black box in Fig. 1). The masking function is given by $M(\mathbf{r})=M(x)M(y)M(z)$, where

$$M(z)=\begin{cases}\cos^{1/8}\left(\frac{\pi|z-z_b+L|}{2L}\right), & |z_b-z|<L\\ 1, & \text{otherwise},\end{cases} \qquad (4)$$

as originally reported by Krause *et al.* [38] and which describes well the absorption in photoemission from atoms subjected to intense laser fields. Here z_b is the boundary either at $z_{\min}$ or $z_{\max}$ in the z axis, with similar expressions for the x and y case, and L is the absorbing width of region Ω. After each time step in the Crank-Nicholson approach, the wave function is multiplied by Eq. (4) to force the electron density to be absorbed at the edge of the grid [37].

The uniform grid employed in the calculations covered the region $[-18,18]_x\times[-18,18]_y\times[-18,18]_z$ a.u. with a grid step of 0.4 a.u., giving $E_H=-0.490$ a.u. for the hydrogen ground state energy. Although this value is not accurate, we argue that it is sufficient to estimate reasonably well the ionization probability, excitation, and energy loss. As an example, in Fig. 2, we show the initial $1s$ electronic density, obtained by an imaginary time propagation of Eq. (2) for the hydrogen at rest, when projecting on x and y, i.e., $\rho(z)=\int dxdy|\Psi(\mathbf{r},t=0)|^2$. The analytical result for a hydrogen atom is obtained by using the $1s$ ground state wave-function, $\Psi=e^{-r}/\sqrt{\pi}$, such that $\rho(z)=(1+2|z|)e^{-2|z|}/2$, shown in Fig. 2 by the solid line, while the symbols are our grid results. Note the good agreement of our numerical approach to that of the analytical solution.

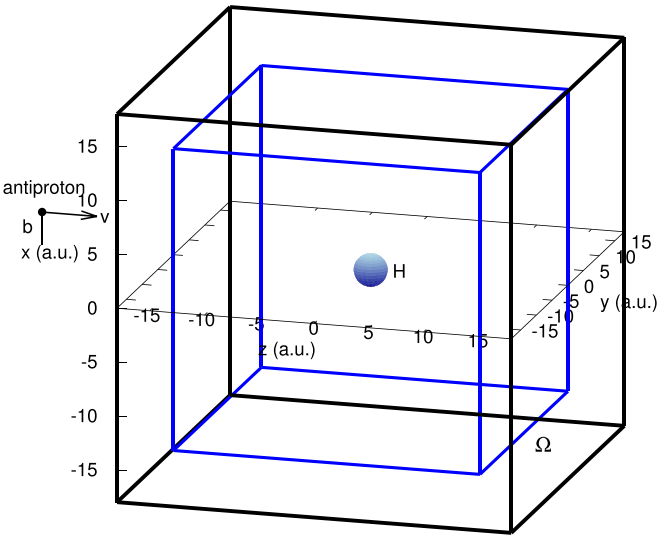

FIG. 1. $\bar{p}$ +H collision rendering. The sphere represents the $1s$ hydrogen electron density, b is the collision impact parameter of an antiproton located initially at a distance z_0, and v is the initial collision velocity. The space between the inner and outer box represents the ionization absorbing region Ω. See text for details.

The calculation time for the propagation is chosen to be long enough to achieve a clear separation at the final time

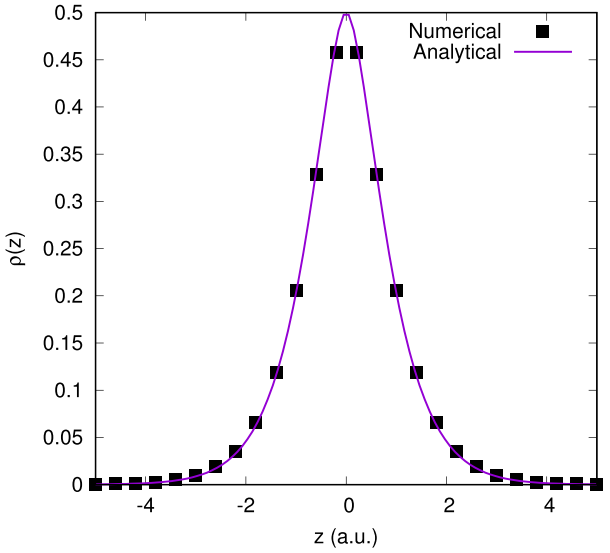

FIG. 2. Initial $1s$ electronic density $\rho(z)$ as a function of z. The solid squared symbols are our numerical results and the solid line is the $1s$ analytical solution. See text for discussion.

between the target and the projectile or to achieve two or three orbits for the formation of Pn. The minimum time t_0 is chosen as $t_0 = z_0/v$, with v the initial antiproton collision velocity, such that $t = 0$ corresponds to the closest collision distance. We have employed a time step of 0.01 a.u., which gives a reasonable compromise between accuracy and computation time. With this time step, Eq. (3) is solved with a fourth-order Runge-Kutta method coupled to Eq. (2). The impact parameter grid was chosen such that the projectile and target have trajectories at the center of a square defined by adjacent points in the xy plane, as suggested in Ref. [36], to avoid numerical instabilities when $\mathbf{R}_i$ passes nearby a grid point $\mathbf{r}$. With this grid step and the restrictions on b on the grid, the impact parameter grid is also in steps of 0.4 a.u. from $b = 0.0$ to $b = 10.0$ a.u. Initially, we place the antiproton on the z axis at a distance of $z_0 = -30$ a.u. and it impinges with an initially velocity commensurate with the collision energy, as shown in Fig. 1. We report calculations for collision energies in the laboratory frame E_p of 3, 5, 10, 20, 24, 26, 28, 30, 50, and 100 eV, as well as to 0.25, 0.5, 0.9, 1.5, 5, 10, 25, 50, 100, 225, 400, and 900 keV. To account for the polarization effects of the antiproton initial finite distance on the hydrogen electronic cloud when placed at $z_0 = -30$ a.u. and $x = b$, the initial wave function in Eq. (2) is calculated by means of the imaginary time technique for each initial configuration. The absorbing width used in the present calculations is $L = 4.0$ a.u., which ensures a proper absorbing layer [37].

III. RESULTS

A. Ionization probability

In an antiproton-hydrogen interaction, the repulsion between the hydrogen electron and the antiproton produces the ionization as a function of the impact parameter and collision energy. We use the masking function, Eq. (4), to describe the absorption process as the electron leaves the numerical box. The probability of finding the electron within the box is given by the norm of the remaining electronic wave function within the box, i.e., $N_e = \langle\Psi(t)|\Psi(t)\rangle$. Consequently, the ionization probability is determined as $P_i = 1 - N_e$. In Fig. 3, we show the norm of the wave function as a function of the collision time for two collision energies. In Fig. 3(a), we show the case for three impact parameters at a collision energy of 100 keV, corresponding to near the maximum of the ionization cross section. The three parameters allow us to study the ionization process for small b, an intermedium impact parameter, and an impact parameter where ionization becomes minimal. In Fig. 3(b), we show the case for a lower collision energy of 500 eV. We observe that after the collision occurs, the norm of the electron wave function has an exponential decay for all impact parameters. As the calculation time of the collision stops at a finite time, the system has not reached the final norm of the wave function. To determine the final ionization probability, we fit the numerical data to a norm that has the form

$$N_e = \beta e^{-\alpha t} + N_{et}. \tag{5}$$

Consequently, when $t \to \infty$, the final norm of the electron wave function is N_{et} and the final ionization probability is then

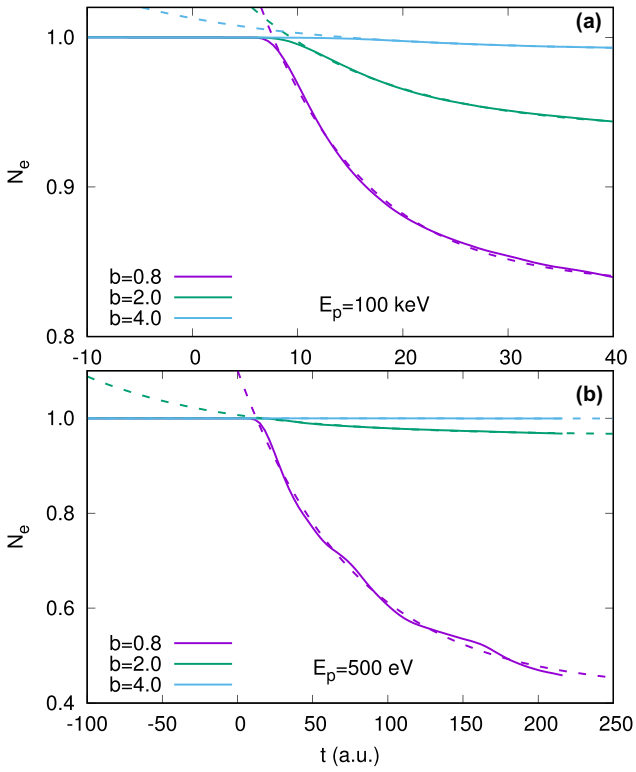

FIG. 3. Norm of the electronic wave function, as a function of the collision time for three different impact parameters ($b = 0.8$, $b = 2.0$, and $b = 4.0$ a.u.) for (a) $E_p = 100$ keV and (b) $E_p = 0.5$ keV collision energy. The solid lines correspond to our numerical dynamics. The dashed lines are the results of Eq. (5). See text for detail.

$P_i = 1 - N_{et}$. In Fig. 3, the results of Eq. (5) are shown by the dashed lines.

From the ionization probability results, we observe that for small impact parameters, the decay in the norm of the wave function oscillates around the exponential envelope. To understand this behavior, we show in Fig. 4 a few frames for the collision dynamics of an antiproton colliding at 500 eV/amu with a hydrogen atom at an impact parameter of $b = 0.8$ a.u. The heat color map represents the electron density projected over the y coordinate. Blue represents no electronic density, red is the maximum electronic density, and white is the intermediate electronic density. The antiproton is represented by the $\oplus$ symbol, the proton in the hydrogen atom is represented by the $\otimes$ symbol, and the $+$ symbol represents the center of mass of the $\bar{p} + p$ system. At time -110.2 a.u. the antiproton is at 15.6 a.u. of distance from the hydrogen atom and the electronic wave function starts to polarize by the antiproton approach. The ionization process starts when the antiproton has reached a closer distance to the hydrogen such that the repulsion between the electron and the antiproton is enough to push the electron into the continuum, as the antiproton is too heavy. This is observed at time -4.2 a.u., which corresponds to a distance of $d = 1.0$ a.u. between the antiproton and the proton. From this time forward, the momentum transfer from the antiproton into the electron cloud induces a spiraling outward process characteristic of angular momentum transfer

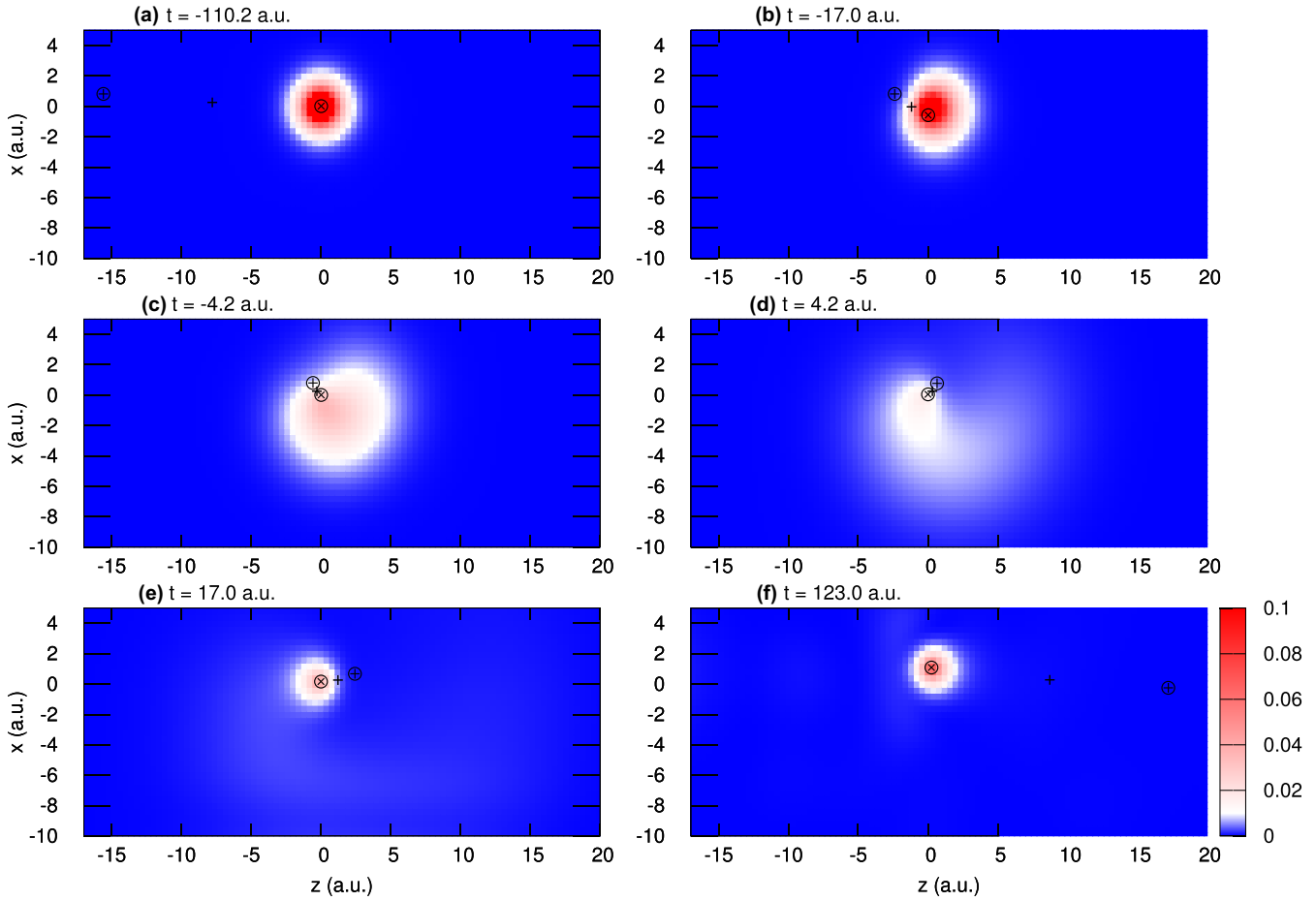

FIG. 4. Collision dynamics for $\bar{p} + \mathrm{H}$ at 0.5 keV and $b = 0.8$ a.u. Here, $\oplus$ is the $\bar{p}$ position, $\otimes$ is the proton position, and $+$ is the position of the center of mass of the $\bar{p} + p$ system. Notice the $\bar{p}$ attractive trajectory and the motion of the remaining hydrogen atom after the closest approach. The color map represents the electron density where blue means no electron density and red high electron density with white intermediate values, as shown by the heat map color box in (f). See text for discussion.

into the electron. This is observed at time 4.2 a.u. and proceeds with several turns around the hydrogen atom consequence of the angular momentum absorbed by the electron. The tail observed in the electronic density carries away the electron, producing the ionization process. In an orbital representation, this wave-tail structure is represented by a linear combination of all the excited states (linear combination of atomic orbitals, LCAO) in the hydrogen atom for bound and continuum states, which requires high angular momentum wave functions to describe well the localized shape in coordinate space, as observed in Fig. 4. In a grid, the final wave-tail structure is well represented within the numerical box. This spiraling tail, which goes away each time it swings around, produces oscillatory behavior in the norm of the wave function, as noticed in Fig. 3. At time 123 a.u. the system is well separated and the ionization process swings down. Notice the change in the trajectory of the center of mass due to momentum carried away by the ionized electron through the coupling of the electron-nuclear dynamics. As the antiproton is attracted by the proton, its scattering angle is negative. The scattering angle is determined by the angle between the initial and final antiproton velocity, i.e., $\theta = \cos^{-1}(\mathbf{v}_i \cdot \mathbf{v}_f / v_i v_f)$ such that if the velocity component along the direction of the impact parameter is positive it represents repulsion (positive scattering angle) and if it is negative it is attraction (negative scattering angle). The change in the angle of the center of mass determines the most probable scattering angle of the ionized electron. Also, note that the hydrogen atom drifts upwards due to the attraction (polarization) from the antiproton from conservation of total angular momentum. All of these results are a consequence of the electron-nuclear coupling described by Eqs. (2) and (3). Interestingly, we notice that this behavior occurs for all collision energies for impact parameters $b < 2$ a.u. As proposed by Fermi and Teller [39], there is a distance at which the electron is no longer bound by the hydrogen atom. To assess this behavior properly, we show in Fig. 5 the electronic energy of the system $\bar{p} + p + e^-$ as a function of the distance R between the $\bar{p}$ and p nuclei, in a static calculation, within the same grid approach, in an imaginary time propagation of Eq. (2). We observe that at a distance $R_c = 1.1$ a.u. the electron is not bound anymore, and in the inset we observe the electron density showing precisely the polarization or repulsion induced by the heavy antiproton on the electron. Here, we show the electron density projected on x

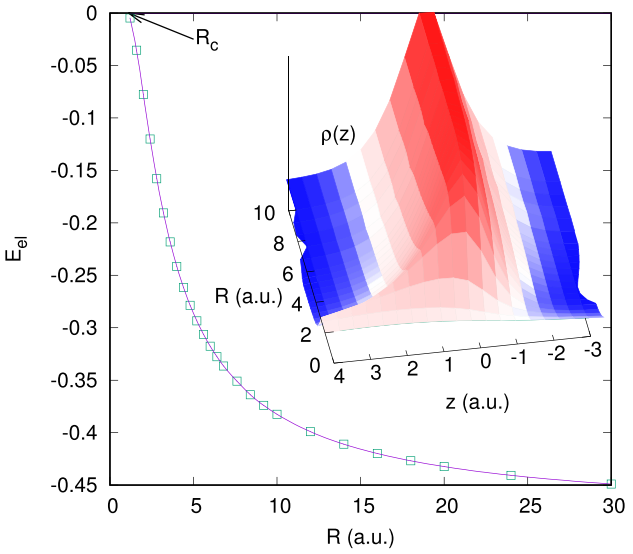

FIG. 5. Electronic ground state energy of the system $\bar{p}+\mathrm{H}$ as a function of the proton-antiproton distance R, as obtained by the imaginary time approach to Eq. (2). The delocalization of the electron occurs at $R_c = 1.1$ a.u. in our numerical grid. In the inset, we show the polarization effect induced by the antiproton on the electron as it approaches the hydrogen atom when placed at a distance R on the negative z axis by showing $\rho(z)$ as a function of z for each R. The color map is the same as in Fig. 4. See text for discussion.

and y as a function of z, and the antiproton is placed in the negative z region, as shown in Fig. 2. Consequently, R_c becomes the critical distance to replace the electron, becoming the so-called Fermi-Teller distance [39], R_{FT}. Fermi and Teller report a value of $R_{\mathrm{FT}} = 0.639$ a.u. obtained as simply the minimum electric dipole moment required to bind an electron, and it is also the internuclear separation where the Born-Oppenheimer approximation breaks down for antiproton-hydrogen scattering. From Fig. 5, our result gives the critical distance as $R_c = 1.1$ a.u., which agrees with the previous discussion of the dynamics and provides a much better description of the physics, as reported below.

Our previous discussion is reinforced when analyzing the ionization probability as a function of the impact parameter. In Fig. 6, we show the ionization probability, weighted by the impact parameter bP_i. In Fig. 6(a), we show our results for 0.1, 5, and 100 keV (solid lines) and compare to the theoretical results of Abdurakhmanov *et al.* [34] (dashed lines) and Sahoo *et al.* [33] (short-dashed lines). Our results are, on average, 10% lower than those of Abdurakhmanov *et al.* due to the electron and nuclei coupling dynamics and the fact that Abdurakhmanov *et al.* use effective potentials. In Fig. 6(b), we show our results for all the collision energies from 0.03 to 900 keV, which are above the maximum energy at which the protonium formation occurs. We observe that the largest contribution occurs for the impact parameter region $0 < b < 2$ a.u. and as the antiproton collision energy is reduced, it tends towards a centralized region (ridge) around $b \sim 1.1$ a.u., in agreement with the Fermi-Teller criteria with our value of R_c. For high collision energies, the ionization region increases toward larger impact parameter consequence of larger momentum transfer.

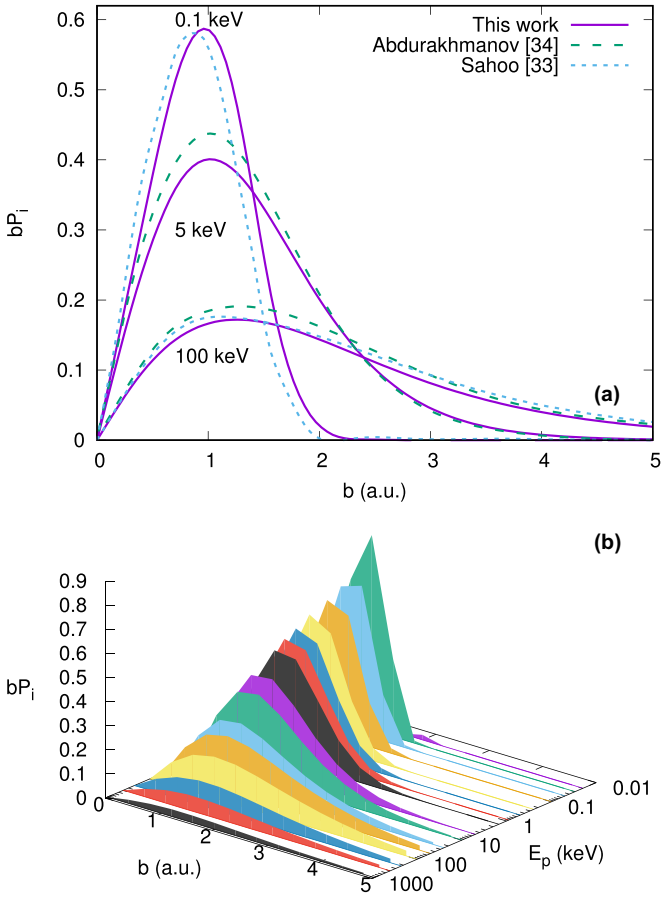

FIG. 6. Ionization probability for $\bar{p}+\mathrm{H}$ as a function of the impact parameter and collision energy. In (a), we show our results for 0.1, 5, and 100 keV (solid line) and compare to the theoretical data of Abdurakhmanov *et al.* [34] (dashed line) and Sahoo *et al.* [33] (short-dashed line). In (b), we show our results for all the energies considered in this work. Notice the ridge around $b \sim 1.1$ a.u. See text for discussion

B. Ionization cross section

The area under the curves of Fig. 6 is proportional to the ionization cross section, since

$$\sigma_i = 2\pi \int bP_i \, db. \tag{6}$$

In Fig. 7(a), we show the ionization cross section as a function of the antiproton collision energy. In the same figure, we compare to the experimental data of Knudsen *et al.* [41] (open square symbols), obtained for antiprotons colliding with molecular hydrogen, and the theoretical results of Schultz *et al.* [28,29], Wells *et al.* [31], Hall *et al.* [32], Abdurakhmanov *et al.* [34], Winter [27], Sakimoto [15–18], Sahoo *et al.* [33], Tong *et al.* [30], and Cohen classical trajectory Monte Carlo (CTMC) [21]. In the same figure, we show the value obtained by using the Fermi-Teller criteria, with $R_c = 1.1$ a.u., shown by the light blue horizontal dotted line. The agreement between our approach and Sakimoto is very good. In the limit of low collision energies, above the maximum energy at which the protonium formation occurs, it tends to the Fermi-Teller limit. At high collision energies, all

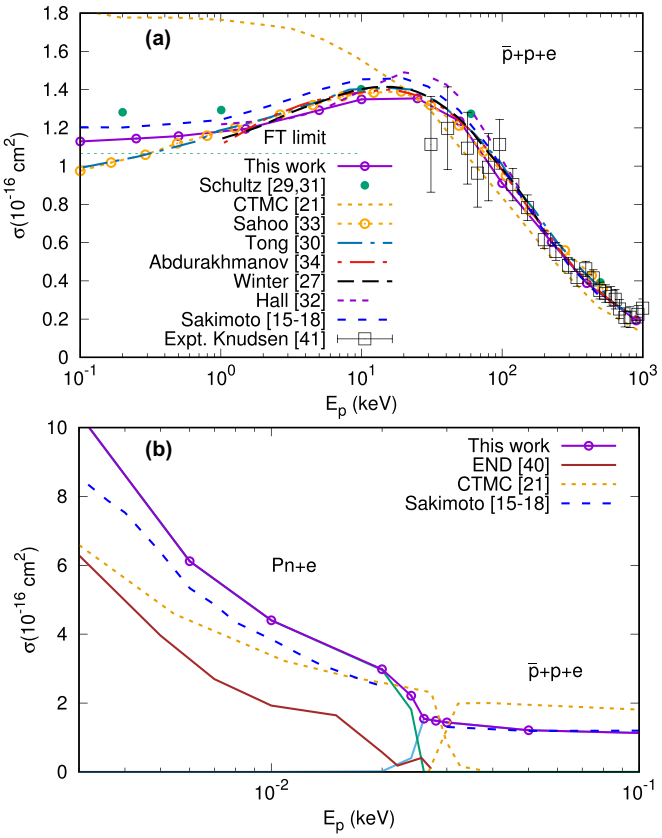

FIG. 7. (a) Ionization cross section for $\bar{p}$ colliding with atomic H as a function of the antiproton kinetic energy. The purple solid line with open circles is the result of our approach and we compare to the theoretical work of Cohen (CTMC) [21] (short dashed orange line), Schultz *et al.* [29,31] (green filled circles), Hall *et al.* [32] (triple-dashed purple line), Abdurakhmanov *et al.* [34] (double-dot dashed red line), Winter [27] (long dashed black line), Sakimoto [15–18] (short-dashed blue line), Tong *et al.* [30] (double dashed-dot green line), Sahoo *et al.* [33] (orange short dashed with open circles line), and END [40] (brown solid line). The light blue dotted line corresponds to the Fermi-Teller limit for our value of $R_c = 1.1$ a.u. The experimental data are from Knudsen *et al.* [41] for molecular H (open square symbols). (b) Protonium formation ($\bar{p}p + e$, solid green line) and ionization ($\bar{p} + p + e$, solid light blue line) cross section for $\bar{p}$ colliding with atomic H as a function of the antiproton kinetic energy. The lines labels are the same as in (a). See text for discussion.

the approaches tend to agree, but at low collision, Cohen's CTMC approach [21] shows a large discrepancy (shown by the short-dashed orange line).

C. Protonium formation

In Fig. 7(b), we show the contribution to the ionization cross section induced by the collision of antiprotons with atomic hydrogen in the low energy collision region down to 27.2 eV in the laboratory frame. This energy, in the relative frame, compares to the hydrogen ionization energy of 13.6 eV. This means that the channel for total break-up opens at this energy, and when it is allowed it is favored over Pn formation. For collision energies between 20 and 27.2 eV (10–13.6 eV in the relative frame), we find that both the protonium formation and collision-induced ionization channels compete. The protonium formation occurs at small impact parameters, in agreement with the Fermi-Teller criteria, while at larger impact parameters the antiproton does not bind. As the collision energy decreases below 20 eV, the dominant channel for ionization is protonium formation, as observed in Fig. 7(b). The solid light blue line is the ionization induced by collision and the solid green line the protonium formation. The total ionization cross section at low collision energy is shown by the purple solid line with open circles. In the same figure, we compare to the results of the CTMC approach reported by Cohen [21], the quantum mechanics discrete variable representation (QM-DVR) results of Sakimoto [15–18], and the END results [40], showing a good agreement when compared to the QM-DVR results.

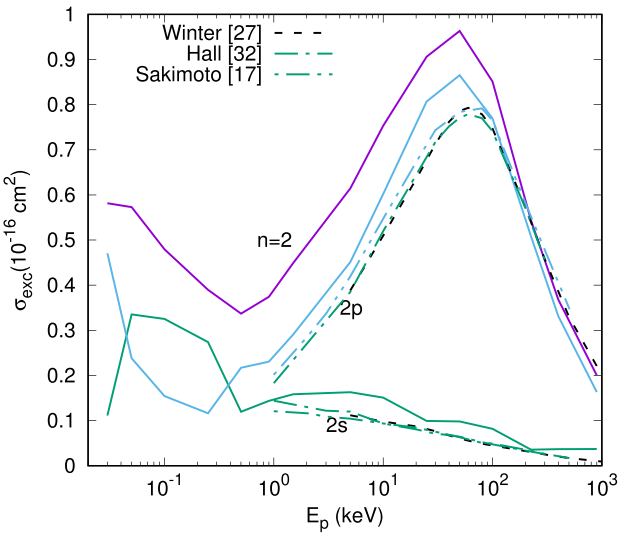

FIG. 8. Hydrogen electronic excitation cross section for the $2s$ and $2p$ states as a function of the antiproton collision energy. The solid lines are our numerical results, while the black dashed line corresponds to the theoretical results of Winter [27], the dashed-dot line is Hall *et al.* [32], and the double dot-dashed line is Sakimoto [17]. See text for discussion.

D. Excitation cross section

By projecting the final wave function into the hydrogenic $2s$, $2p_{-1}$, $2p_0$, and $2p_1$ states, we determine the hydrogen excitation probability. In Fig. 8, we show the excitation cross section for the $2s$ and $2p$ states of hydrogen as a function of the antiproton collision energy and compare to the theoretical results reported by Winter [27], Hall *et al.* [32], and Sakimoto [17]. We find that our results are, on average, 10% higher than those of Winter, Hall *et al.*, and Sakimoto. As discussed previously, the ionization shows an exponential decay that has not reached its final value. Consequently, the excitation probability follows a similar trend. In this case, we have not corrected our results for that effect. In general, our agreement is fairly good and gives us confidence that our numerical approach captures properly the physics of the collision dynamics. Interestingly, the excitation cross section peaks around 50 keV/amu collision energy, confirming that at low collision energies the ionization process is the

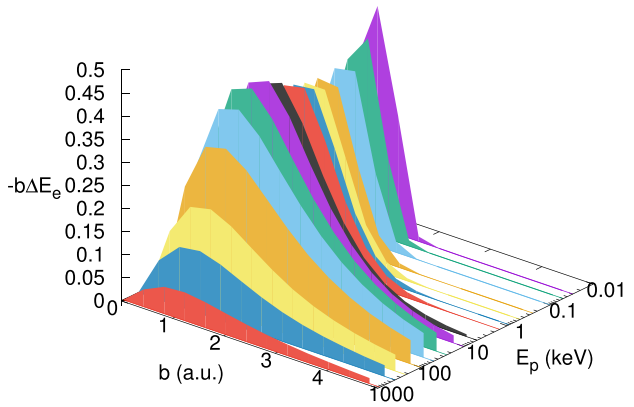

FIG. 9. Electronic energy loss for $\bar{p}$ colliding with atomic H as a function of the impact parameter and collision energy. Notice the ridge around $b \sim 1.1$ a.u. See text for discussion.

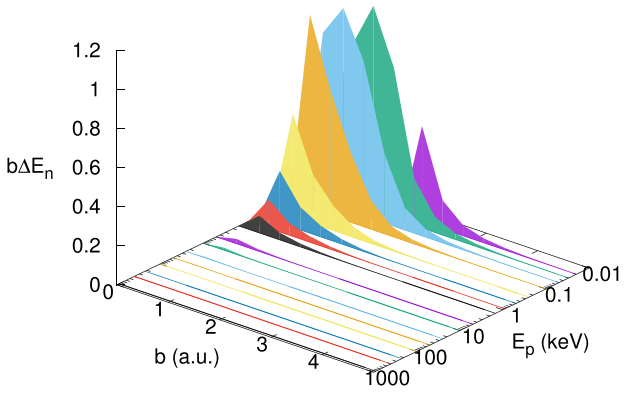

FIG. 10. Nuclear kinetic energy loss of $\bar{p}$ when colliding with atomic H as a function of the impact parameter and collision energy. See text for discussion.

dominant channel and that the excitation increases for collision energies above the maximum energy at which the protonium formation occurs, with a minimum around 500 eV.

E. Antiprotons energy loss

For those trajectories where there is no formation of Pn, that is, the antiproton is not captured by the atomic hydrogen, the energy required to induce the ionization process comes from the kinetic energy loss of the projectile. Then the total projectile energy loss is $\Delta E_t = K_f - K_i$, where K_f and K_i are the final and initial kinetic energy of the antiproton and are given by $K = P_p^2/2M_p$. Here, the final antiproton momentum $\mathbf{P}_p$ is given by Eq. (3) at the end of the dynamics. This energy loss is decomposed into the electronic energy loss in the target frame (excitation-ionization) and an energy loss that goes into target displacements. Thus, the electronic energy loss is $\Delta E_e = K_f^r - K_i^r$ with $K^r = p_r^2/2\mu_p$, where p_r is the momentum of a projectile with reduced mass $\mu = M_p/2$. In Fig. 9, we show the electronic energy loss, weighted by the impact parameter, as a function of the initial antiproton energy and impact parameter. By comparing to the results of Fig. 6, the correlation between the ionization process and the projectile electronic energy loss is observed, i.e., the projectile loses kinetic energy that goes into the target and induces the ionization process for the same region of impact parameters. However, the energy loss of the projectile also goes into displacing the hydrogen atom, that is, the target recoils due to the momentum transferred by the projectile. As the hydrogen atom momentum is also given by Eq. (3) and since it is initially at rest, the energy gained by the target displacement as nuclear recoil gives the nuclear energy loss, $\Delta E_n = P_t^2/2M_t$, where $\mathbf{P}_t$, is given by Eq. (3), as the target final momentum. The total energy loss is given by the sum of these two contributions. In Fig. 10, we show the target nuclear energy gain, weighted by the impact parameter, as a function of the projectile kinetic energy and impact parameter. At high collision energies or large impact parameters, the target recoil is very small. At low projectile collision energies, the target kinetic energy increases for low impact parameters due to polarization effects induced by the antiproton on the hydrogen target.

Once the electronic energy loss is determined, the electronic stopping cross section is calculated by

$$S_e(E_p) = 2\pi \int b\Delta E_e \, db, \tag{7}$$

and the nuclear stopping cross section is given by replacing ΔE_e by ΔE_n.

In Fig. 11, we show the stopping cross section for antiprotons colliding with atomic hydrogen. In the same figure, we compare with the experimental data reported by Adamo *et al.* [5] obtained for a molecular hydrogen target and to the theoretical results of Bailey *et al.* [42] convergent close-coupling

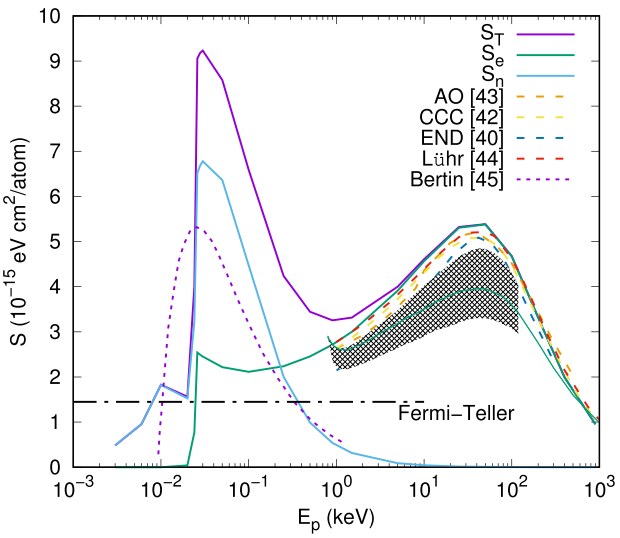

FIG. 11. Stopping cross section for $\bar{p}$ colliding with atomic hydrogen as a function of the initial antiproton kinetic energy. Purple solid line is the antiproton total stopping cross section. Green solid line is the electronic stopping cross section and the light blue solid line is the nuclear stopping cross section. We compare to the theoretical results of Bailey *et al.* [42] (CCC), Schiwietz *et al.* [43] (AO), Lühr and Saenz [44], and the electron-nuclear dynamics [40] (END), for the electronic stopping cross section. The shaded area is the experimental data from Adamo *et al.* [5] for $\bar{p}$ colliding with H_2. The short dashed line is the nuclear stopping cross section for $\bar{p}$ on molecular H obtained experimentally by Bertin *et al.* [45] through a Rutherford cross section. See text for discussion.

(CCC), Schiwietz *et al.* [43] atomic orbitals (AO), Lühr and Saenz [44], and the electron-nuclear dynamics [40] (END). We find that our approach accounts well for the antiproton energy deposition into the electronic and nuclear degrees of freedom of the hydrogen target, as our results compare well with the other theoretical calculations. The electronic stopping cross section peaks at $E_p \sim 50$ keV and presents a minimum at $E_p \sim 100$ eV with a sudden drop at the energy at which the protonium formation ceases. The nuclear stopping cross section starts to contribute below $E_p \sim 10$ keV and presents a peak at $E_p \sim 30$ eV with a sudden drop around the energy at which the protonium formation channel closes. Furthermore, we find that at low collision energies, the dominant channel is the nuclear target recoil, although the ionization process still has a large contribution. This is due to the large mass difference between the ionized electron and the target nuclear mass. For collision energies above 27.2 eV, in the laboratory frame, there is no formation of protonium and all the impact parameters contribute to the energy loss process. For collision energies below the energy at which the protonium formation closes, we only consider those impact parameters that do not bind to determine the energy loss. This is shown in Fig. 11 by the abrupt change in the energy loss at the energy at which the protonium formation channel closes. The small bump around $E_p \sim 10$ eV is the contribution of trajectories that do not bind and slow down the projectile due to the polarization of the hydrogen electronic cloud, with the attraction of the proton-antiproton. Those trajectories that form Pn are not accounted for in the energy loss process. In the same figure, we show the Fermi-Teller criteria, i.e., for $b \leqslant R_c$, the minimal energy transferred to the target is the ionization potential, $I_H = 13.6$ eV such that the Fermi-Teller minimal energy loss is $S_e^{\mathrm{FT}} = \pi R_c^2 I_H/2$, which is shown by the horizontal short dashed line. In the same figure, we show the nuclear stopping cross section reported by Bertin *et al.* [45] obtained through a Rutherford cross section (short-dashed line). At $E_p \sim 1$ keV Bertin *et al.* and our nuclear stopping cross section agree, but as the collision energy is reduced, the results differ. The results of Bertin *et al.* do not take into account the protonium formation, show a smooth profile, and are obtained for molecular H.

IV. CONCLUSIONS

We have carried out a time-dependent solution to the Schrödinger equation for a hydrogen atom in a collision with an antiproton by including the electron-nuclear coupling into the dynamics in a numerical grid. With this, we determine the ionization, excitation, protonium formation, and stopping cross sections for the system $\bar{p} + \mathrm{H}$. Our results show that the dominant channel is the ionization process and it is well described by the Fermi-Teller criteria at low collision energies. The Fermi-Teller distance is corrected to the critical radius $R_c = 1.1$ a.u. by calculating the delocalization of the electron as a function of the antiproton-proton distance. The Fermi-Teller criteria describes reasonably well the ionization and energy-loss processes in the region where its assumptions are valid. We confirm that at low collision energies, the nuclear energy loss is dominant and is a consequence of the polarization attraction between the antiproton and the hydrogen atom. Finally, our approach describes very well the protonium formation cross section and distinguishes between the antiproton capture and pure ionization of the electron. At high collision energies, our numerical results agree well with available experimental data and other theoretical approaches. When extending to low collision energy, it becomes evident that our predictions require experimental confirmation.

We hope our results encourage further interest from the experimental community to confirm our findings at low collision energy where the nuclear stopping cross section is larger than the electronic and the protonium formation is dominant compared to the high collision energy region.

ACKNOWLEDGMENTS

R.C.-T. acknowledges support from Grants No. UNAM-DGAPA-PAPIIT IN-109-623, No. 111-820, and No. LANCAD-UNAM-DGTIC-228, as well as to the University of Goteborg for providing the conditions for a visiting stay where this work was concluded.

[1] S. P. Møller, E. Uggerhøj, H. Bluhme, H. Knudsen, U. Mikkelsen, K. Paludan, and E. Morenzoni, Phys. Rev. A **56**, 2930 (1997).
[2] S. Møller, E. Uggerhøj, H. Bluhme, H. Knudsen, U. Mikkelsen, K. Paludan, and E. Morenzoni, Nucl. Instrum. Methods Phys. Res., Sect. B **122**, 162 (1997).
[3] E. Widmann (ASACUSA), Tech. Rep., CERN, Geneva (2018), https://cds.cern.ch/record/2300138.
[4] CERN PS 194, Tech. Rep., CERN, Geneva (1986), https://cds.cern.ch/record/679910.
[5] A. Adamo, M. Agnello, F. Balestra, G. Belli, G. Bendiscioli, A. Bertin, P. Boccaccio, G. C. Bonazzola, T. Bressani, M. Bruschi *et al.*, Phys. Rev. A **47**, 4517 (1993).
[6] G. Gabrielse, A. Khabbaz, D. S. Hall, C. Heimann, H. Kalinowsky, and W. Jhe, Phys. Rev. Lett. **82**, 3198 (1999).
[7] G. Gabrielse, N. S. Bowden, P. Oxley, A. Speck, C. H. Storry, J. N. Tan, M. Wessels, D. Grzonka, W. Oelert, G. Schepers *et al.* (ATRAP Collaboration), Phys. Rev. Lett. **89**, 233401 (2002).
[8] P. Indelicato, Phys. Scr. **2004**, 20 (2004).
[9] B. Gato-Rivera, *Experiments with Antiatoms* (Springer International Publishing, Cham, 2021), pp. 231–252.
[10] T. Yamazaki, N. Morita, R. S. Hayano, E. Widmann, and J. Eades, Phys. Rep. **366**, 183 (2002).
[11] J. Eades and F. J. Hartmann, Rev. Mod. Phys. **71**, 373 (1999).
[12] S. Jonsell, Philos. Trans. R. Soc. A **376**, 20170271 (2018).
[13] M. Doser, Prog. Part. Nucl. Phys. **125**, 103964 (2022).
[14] T. Kirchner and H. Knudsen, J. Phys. B: At. Mol. Opt. Phys. **44**, 122001 (2011).
[15] K. Sakimoto, J. Phys. B: At. Mol. Opt. Phys. **33**, 3149 (2000).
[16] K. Sakimoto, J. Phys. B: At. Mol. Opt. Phys. **34**, 1769 (2001).

[17] K. Sakimoto, J. Phys. B: At. Mol. Opt. Phys. **33**, 5165 (2000).
[18] K. Sakimoto, Phys. Scr. **2004**, 271 (2004).
[19] J. S. Cohen, R. L. Martin, and W. R. Wadt, Phys. Rev. A **24**, 33 (1981).
[20] J. S. Cohen, Phys. Rev. A **36**, 2024 (1987).
[21] J. S. Cohen, Phys. Rev. A **56**, 3583 (1997).
[22] J. S. Cohen, Phys. Rev. A **59**, 1160 (1999).
[23] J. S. Cohen, Rep. Prog. Phys. **67**, 1769 (2004).
[24] K. Ohtsuki, Y. Ishida, M. Matsuzawa, and M. Shinada, in *XXI ICPEAC: 21st International Conference on the Physics of Electronic and Atomic Collisions*, edited by Y. Itikawa (Tokyo, 1999), p. 438.
[25] B. D. Esry and H. R. Sadeghpour, Phys. Rev. A **67**, 012704 (2003).
[26] M. Hesse, A. T. Le, and C. D. Lin, Phys. Rev. A **69**, 052712 (2004).
[27] T. G. Winter, Phys. Rev. A **83**, 022709 (2011).
[28] D. R. Schultz, Phys. Rev. A **40**, 2330 (1989).
[29] D. R. Schultz, P. S. Krstić, C. O. Reinhold, and J. C. Wells, Phys. Rev. Lett. **76**, 2882 (1996).
[30] X.-M. Tong, T. Watanabe, D. Kato, and S. Ohtani, Phys. Rev. A **64**, 022711 (2001).
[31] J. C. Wells, D. R. Schultz, P. Gavras, and M. S. Pindzola, Phys. Rev. A **54**, 593 (1996).
[32] K. A. Hall, J. F. Reading, and A. L. Ford, J. Phys. B: At. Mol. Opt. Phys. **29**, 6123 (1996).
[33] S. Sahoo, S. C. Mukherjee, and H. R. J. Walters, J. Phys. B: At. Mol. Opt. Phys. **37**, 3227 (2004).
[34] I. B. Abdurakhmanov, A. S. Kadyrov, I. Bray, and A. T. Stelbovics, J. Phys. B: At. Mol. Opt. Phys. **44**, 075204 (2011).
[35] E. Deumens, A. Diz, R. Longo, and Y. Öhrn, Rev. Mod. Phys. **66**, 917 (1994).
[36] F. Anis, V. Roudnev, R. Cabrera-Trujillo, and B. D. Esry, Phys. Rev. A **73**, 043414 (2006).
[37] U. De Giovannini, A. H. Larsen, and A. Rubio, Eur. Phys. J. B **88**, 56 (2015).
[38] J. L. Krause, K. J. Schafer, and K. C. Kulander, Phys. Rev. A **45**, 4998 (1992).
[39] E. Fermi and E. Teller, Phys. Rev. **72**, 399 (1947).
[40] R. Cabrera-Trujillo, J. R. Sabin, Y. Öhrn, and E. Deumens, Phys. Rev. A **71**, 012901 (2005).
[41] H. Knudsen, U. Mikkelsen, K. Paludan, K. Kirsebom, S. P. Møller, E. Uggerhøj, J. Slevin, M. Charlton, and E. Morenzoni, Phys. Rev. Lett. **74**, 4627 (1995).
[42] J. J. Bailey, A. S. Kadyrov, I. B. Abdurakhmanov, D. V. Fursa, and I. Bray, Phys. Rev. A **92**, 022707 (2015).
[43] G. Schiwietz, U. Wille, R. Díez Muiño, P. Fainstein, and P. Grande, Nucl. Instrum. Methods Phys. Res., Sect. B **115**, 106 (1996).
[44] A. Lühr and A. Saenz, Phys. Rev. A **79**, 042901 (2009).
[45] A. Bertin, M. Bruschi, M. Capponi, I. D'Antone, S. De Castro, A. Ferretti, D. Galli, B. Giacobbe, U. Marconi, M. Piccinini *et al.*, Phys. Rev. A **54**, 5441 (1996).